Andean Geology 48 (3): 529-545. September, 2021
doi: 10.5027/andgeoV48n3-3256

Andean Geology
www.andeangeology.cl

The likely Quaternary active El Arrayán fault, Santiago, Chile

José Araya[1], *Gregory P. De Pascale[1], Rodrigo Mardel[1], Sergio A. Sepúlveda[1, 2, 3]

[1] Departamento de Geología, Universidad de Chile, Plaza Ercilla 803, Santiago.
j.arayazuleta@gmail.com; snowyknight@gmail.com; rodrigo.mardel@ug.uchile.cl; ssepulveda@ing.uchile.cl
[2] Instituto de Ciencias de la Ingeniería, Universidad de O´Higgins, Libertador Bernardo O'Higgins 611, Rancagua.
[3] Currently at Department of Earth Sciences, Simon Fraser University, 8888 University Drive, Burnaby, B.C., V5A 1S6, Canada.

** Corresponding author: snowyknight@gmail.com*

ABSTRACT. Understanding the location and nature of Quaternary active crustal faults is critical to the reduction of both fault rupture and strong ground motions hazards in built environments. Recent work along the San Ramón Fault (SRF) demonstrates that crustal seismic sources are important hazards within the Santiago Metropolitan region of Chile. In this paper, we present the evidence of a second likely Quaternary active fault (the El Arrayán Fault, EAF) that runs through the northeastern part of Santiago, in the Lo Barnechea area. The EAF is a strike-slip fault zone at least 13 km-long, has a steep dip (mean dip 77º NNE), and a WNW-ESE general trend (~110º) that cuts across folded rocks of the Abanico Formation and Quaternary deposits. Sequences of meter-wide fault rocks in El Arrayán area are coincident with the tectonic geomorphology of the EAF, with fault scarps, deflected streams, saddles, "island hills", sag ponds and linear valleys in the La Dehesa area and coincident with fault strike from the bedrock exposures. Although direct dating is not yet available, fault exposures tied to fault-related tectonic and geomorphic features that crosscut Late-Quaternary morphologies and deposits (including hillslopes, ridges, landslides and alluvial fans), provides strong evidence that the EAF is a Quaternary active and seismogenic crustal fault. Sinistral slickensides and left-lateral deflected streams indicates a left-lateral kinematics (with slight up to the north reverse motion) for the EAF. Due to the location, geometry, kinematics and likely Quaternary activity of the EAF, this structure is interpreted as an arc-oblique transfer zone of the West Andean Thrust (WATS). If the EAF has stick-slip behaviour, it is potentially an important source of fault rupture and strong ground motions and could be responsible for earthquakes up to Mw 6.4 based on earthquake scaling laws and microseismicity observations in and around Santiago. The lack of fault zone avoidance criteria (*i.e.,* do not build in and around active faults) in Chilean law, requires immediate enhanced fault mapping, legislation and the implementation of active fault rupture avoidance areas to reduce the risk associated with active crustal structures in the built environment.

Keywords: Neotectonics, Active faults, Seismic hazard, El Arrayán fault, WATS, Santiago, Chile.

RESUMEN. La falla El Arrayán, probablemente activa durante el Cuaternario. Santiago, Chile. Comprender la ubicación y la naturaleza de fallas corticales activas en el Cuaternario es crítico para la reducción de peligros en ambientes edificados, asociados tanto a ruptura de falla como a fuertes movimientos de tierra. Recientes trabajos enfocados en la Falla de San Ramón (FSR) demuestran que fuentes sísmicas corticales presentan importantes peligros en la región metropolitana de Santiago de Chile. En este trabajo presentamos evidencia de una segunda falla cuaternaria (Falla El Arrayán, FEA), posiblemente activa, que corre a través de la parte noreste de Santiago, en lo Barnechea. La FEA es una falla de rumbo, de al menos 13 km de largo, tiene un manteo alto (77° NNE promedio), y una orientación general ONO-ESE (~110º) que corta rocas plegadas de la Formación Abanico y depósitos cuaternarios. Secuencias de rocas de falla de ancho métrico en El Arrayán pueden ser vinculadas con morfologías tectónicas, a través de escarpes de falla, arroyos desviados, "sillas de montar", "cerros islas", "estanques hundidos" y valles lineales en la Dehesa, los cuales coinciden con el rumbo de las exposiciones de fallas en roca. Aunque dataciones directas no están disponibles, exposiciones de falla, vinculadas con características morfológicas y tectónicas relacionadas con fallamiento, que cortan morfologías y depósitos cuaternarios (lo que incluye remociones en masa y abanicos aluviales), proveen fuerte evidencia de que la FEA es una falla cortical cuaternaria activa y sismogénica. Planos de falla sinistrales y arroyos desviados hacia la izquierda indican una cinemática sinistral (con menor movimiento inverso del bloque norte) para la FEA. Debido a la ubicación,

la geometría, la cinemática y posiblemente la actividad cuaternaria de la FEA, esta estructura puede ser interpretada como una zona de transferencia del WATS (West Andean Thrust) oblicua al arco. Si la FEA posee un comportamiento de deslizamiento friccionado tipo *stick-slip*, es potencialmente una importante fuente de ruptura y de fuertes movimientos de tierra, y puede ser responsable de sismos de tamaño hasta Mw 6,4, basado en leyes de escalamiento de sismos y estudios microsísmicos en Santiago y sus alrededores. La falta de criterios para no construir sobre y alrededor de fallas activas en la ley chilena, hace necesario un mapeo de fallas mejorado, como también la implementación de una legislación sobre el establecimiento de áreas de restricción para la construcción de obras civiles en zonas con fallas activas, para así reducir el riesgo en entornos edificados asociado a estructuras activas en la corteza.

Palabras clave: Neotectónica, Fallas activas, Peligro sísmico, Falla El Arrayán, WATS, Santiago, Chile.

1. Introduction

The Andes of Central Chile and Argentina is one of the highest active orogens on Earth with peaks reaching up to 7,000 m high (*e.g.,* Mt Aconcagua, Tupungato volcano), partially controlled by a rapid (6-8 cm/year) tectonic plate convergence (Fig. 1A; Pardo-Casas and Molnar, 1987; DeMets *et al*., 1994; Gripp and Gordon, 2002). Santiago, the Capital City of Chile (with ~7 Million inhabitants) is located at approximately 500 m above sea level immediately to the west of the Central High Andes (Fig. 1A). Although hazards associated with great to giant earthquakes along the plate boundary here are well-known (*e.g.,* Dura *et al*., 2015; Candia *et al*., 2017), the seismic hazard associated with crustal faults is less known. According to historical seismicity record, in September 1958 a strike-slip related moment magnitude (Mw) 6.3 earthquake occurred at a depth of 8 km at Las Melosas, ~60 km to the southeast of Santiago (Fig. 1B; Alvarado *et al*., 2009). This earthquake caused significant damage to hydroelectric plants, a water-supply aqueduct, accompanied by extensive landslides and rock falls in the region (Sepúlveda *et al*., 2008). In spite of the high strong ground motions from this event, no surface ruptures were encountered. This event demonstrates the importance of shallow crustal earthquakes (from the rupture of crustal faults; see De Pascale, 2021) as sources of seismic hazards in the Principal Cordillera and around Santiago. Instrumentally registered earthquakes over the past few decades indicate that the shallow seismicity in the Andes concentrates along two N-S lineaments exposed along the western flank of the Principal Cordillera (~15 km depth) and within the Principal Cordillera (~10 km depth; Fig. 1B; Barrientos *et al*., 2004; Pérez *et al*., 2014; Ammirati *et al*., 2019). However, it should be noted that along many Quaternary active faults, the seismic recurrence takes place over periods of hundreds to tens of thousands of years, something that cannot be captured from relatively short-duration seismic networks records (*e.g*., Schwartz and Coppersmith, 1984). Thus, geological investigations focussed on mapping and active fault characterization remains major goals in seismic hazard assessments.

Numerous geological faults were mapped in the Central Andes around Santiago (Fig. 1B; Thiele, 1980; Wall *et al.,* 1999; Sellés and Gana, 2001; Giambiagi *et al*., 2003; Sernageomin, 2003; Fock, 2005; Armijo *et al*., 2010; Piquer *et al*., 2016, 2017; Riesner *et al*., 2017). However, there is limited information regarding these faults (*e.g*., fault rocks, sense of displacement), nor recency of activity constrained. Most of these structures are Late-Cenozoic in age and are related with the development and later inversion of the Abanico Basin (Charrier *et al*., 2002, 2007). The classic version of the evolution of the Abanico Basin considers the following stages. The Abanico Basin is a former Cenozoic intra-arc extensional basin, which is now inverted and mostly infilled by volcanic, volcaniclastic and sedimentary rocks of the Abanico and Farellones Formations. The basin infill occurred between the Oligocene and Miocene (Charrier *et al*., 2002, 2007; Giambiagi *et al*., 2003; Fock, 2005) as determined by stratigraphic relationships, fossil occurrence, and radioisotopic ages. The tectonic extension of the basin was related with the activity of N-S high-angle regional scale normal faults such as the Los Angeles-Infiernillo, San Ramón, and El Diablo faults mainly located at the edges of the basin during Oligocene (Charrier *et al*., 2002, 2007; Fock *et al*., 2006; Farías *et al*., 2008). These N-S striking regional fault systems also controlled a tectonic basin inversion and exhumation during the Early to Middle Miocene (Giambiagi *et al*., 2003), in which the Abanico Formation was deformed and the Farellones Formation was deposited

(Charrier *et al*., 1996, 2002, 2007). The now inverted N-S regional scale reverse structures are part of the large east-vergent Aconcagua Fold and Thrust Belt tectonic unit (Fig. 1B; Giambiagi *et al*., 2003) and the west-vergent West Andean Thrust System (*i.e.*, WATS; Fig. 1B; Armijo *et al*., 2010). In the internal part of the basin conjugate NW-SE and NE-SW orientated strike-slip structural trends were interpreted based on direct structural observations, regional-scale gravimetry, seismic and magnetic data (Piquer *et al.,* 2016, 2017). Early to Middle Miocene faulting is likely due to compressive deformation during the Abanico Basin inversion (Charrier *et al*., 2005).

To further complicate the history of the Abanico Basin outlined above, new dating and fieldwork (Mosolf *et al*., 2019) from southeast of Santiago (~35° S) provides a robust and older chronostratigraphic framework spanning *ca*. 75-11 Ma. Thus this new work shows the Abanico basin is much older than previously recognized, in which the Late-Cretaceous to Late Eocene intra-arc sedimentation and volcanism which deposited the Abanico Formation, followed by Late Eocene to Late Miocene strike slip dextral shearing within the volcanic arc. Mosolf *et al*. (2019) divides the Abanico Formation into upper and lower, with 37 Ma being the limit between these two divisions. Based on accumulation rates, and other data, they suggest that instead of a fault-bounded basin, the Abanico Formation slowly accumulated in an arc platform. Importantly, based on field mapping and age control Mosolf *et al*. (2019) show that the NW-striking sinistral strike-slip faulting found in the

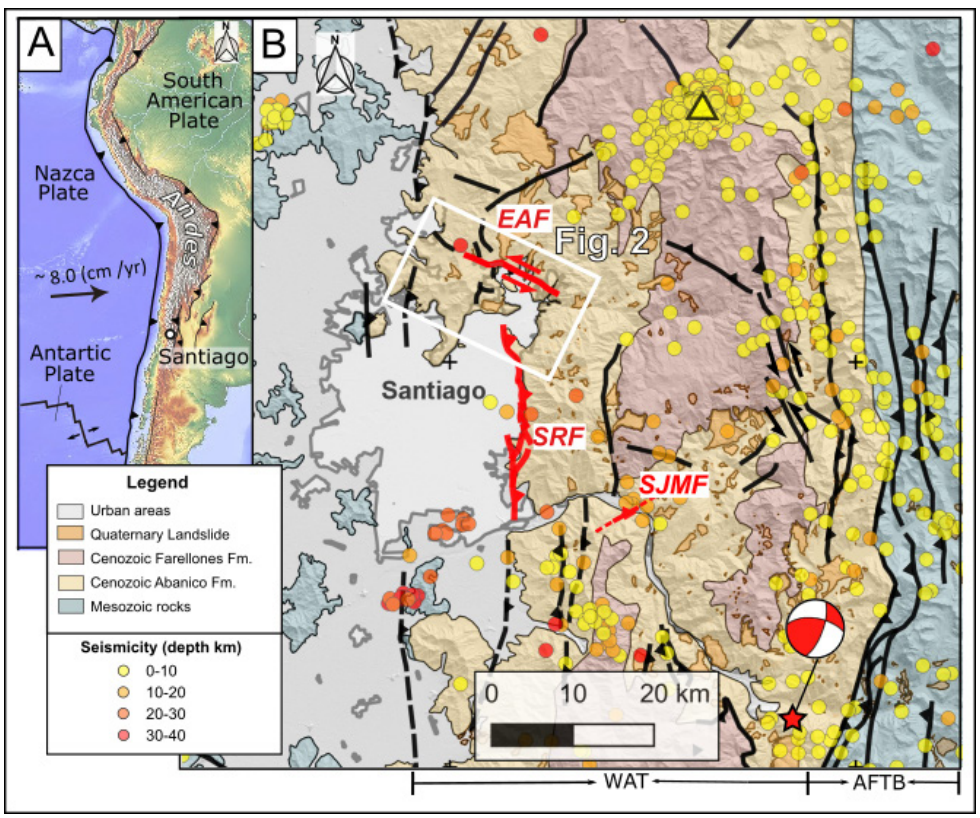

FIG. 1. **A.** Simplified tectonic framework of the subduction margin of the Andes. Black arrow shows tectonic plate convergence velocity (Gripp and Gordon, 2002). Location of the City of Santiago is shown. **B.** Geologic and seismic framework of Santiago and the Principal Cordillera between 33-34° S and the locations of major known or suspected active faults from this study and other authors (see text). Major faults are shown with thick black lines. Active and likely active faults in thick red lines. Seismicity from USGS, where small circles mark the epicenter locations. Red star shows the 1958 Mw 6.3 Las Melosas Earthquake location and focal mechanism (Alvarado *et al*., 2009). White box shows location of figure 2. **EAF**: El Arrayán Fault; **SRF**: San Ramón Fault; **SJMF**: San José de Maipo Fault. **WATS** (West Andean Thrust System); **AFTB** (Aconcagua Fold and Thrust Belt).

Abanico Formation appears to be younger than all other structures in regionally based on cross-cutting relationships. To further complicate the story, Muñoz *et al*. (2009) reports a 38.4 Ma old dike that cuts through folded Cretaceous strata that are unconformably overlain by the Abanico deposits. This would suggest that the Abanico Formation is younger than at least 38.4 Ma.

Additionally, Middle Miocene-Early Pliocene faulting in the Abanico Basin is suggested by syn-tectonic hydrothermal mineral fibers on the NW-striking and NE-striking conjugated strike-slip faults system, under a transpressive regime with E -to ENE- directed shortening (Piquer *et al*., 2015, 2016). Late-Quaternary faulting in Santiago was documented along the San Ramón Fault. The San Ramón Fault is a N-S to NNW-SSE striking, west-vergent reverse fault, that is part of the West Andean Thrust (Armijo *et al*., 2010), with a prominent fault scarp at the foothills of the western flank of the Principal Cordillera, within the limits of urban Santiago, that accommodates part of the compressional stress regime in this sector of the Central Andes (Rauld, 2002, 2011; Armijo *et al.,* 2010; Vargas *et al*., 2014; Estay *et al*., 2016). The fault is well mapped between the Mapocho and Maipo Rivers (Armijo *et al*., 2010; Rauld, 2011). The geometry of the northern part of the SRF is composed of a string of three arch-shaped hills. These hills correspond to eroded remnants of a gentle NW-striking anticline structure, which deforms the Abanico Formation bedrock and the Quaternary sediments (Armijo *et al*., 2010). This anticline, compared with the southern and more regular part of the SRF, is not located immediately to the west of the mountain front. The anticline instead may be indicative of some near-surface complexity in a fault propagation process in the area (Armijo *et al*., 2010). Geophysical evidence as revealed by electrical resistivity and seismic profiling of the SRF supports the presence of the structure at the subsurface (Díaz *et al*., 2014; Pérez *et al*., 2014; Estay *et al*., 2016; Ammirati *et al*., 2019). Wells and Coppersmith's (1994) scaling relationships, allow to estimate a Mw 6.9 earthquake potential for the SRF, based on structural reconstructions (Armijo *et al*., 2010). However, paleo-seismic trenching (Vargas *et al.*, 2014) provides a general first order potential Mw 7.5 earthquake based on earthquake scaling relationships. Some authors suggest that the fault continues to the north at the eastern edge of the Chicureo area, and to the south it is found east of the Pirque area (Armijo *et al.*, 2010; Vargas *et al*., 2014; Estay *et al.*, 2016). Nevertheless, strong evidence of these northern and southern locations of the San Ramón Fault or related structures is not currently available.

The San José de Maipo fault, located 5 km north of the city of San José de Maipo, in which reverse faults and drag folds, of unknown length, were described within Quaternary terraces (Lavenu *et al*., 1994; Lavenu, 2006; Lavenu and Cembrano, 2008). The fault does not have geomorphic expression in the landscape and a map trace length could not be determined (Lavenu and Cembrano, 2008). A NNW shortening direction was determined based on kinematic analysis of mesoscopic fault-slip data of the San Jose de Maipo fault (Lavenu and Cembrano, 2008). Nonetheless, apart from these two faults, the existence of other active crustal seismic sources in or around metropolitan Santiago are still poorly constrained.

Therefore, the development of an accurate seismic hazard assessment and the understanding of fault rupture hazards in the most populated city in Chile, requires recognition and understanding of the active regional crustal seismic sources. This work, characterizes the recently discovered El Arrayán Fault (EAF) in northeastern Santiago.

2. Methods

The EAF was discovered by our research team during a field mapping survey that aimed evaluating potential active faults within urban Santiago in the El Arrayán sector within the Municipality of Lo Barnechea. The presence of numerous road cuts in this sector provided a rare occurrence in urban Santiago to see evidence for faulting and hence this area was a key target. A combined remote sensing analysis and fieldwork was performed in order to document and characterise the EAF beyond the key outcrop in El Arrayán. Lithological, structural data and geomorphological observations were documented during fieldwork (Fig. 2A-D; Fig. 3A-E). Activities such as rock sampling and description, structural measurements, determination of kinematic indicators and photographic documentation allowed the characterisation of the EAF. Subsequent field mapping allowed tracking the tectonic geomorphology of the EAF west of El Arrayán, where it crosses the

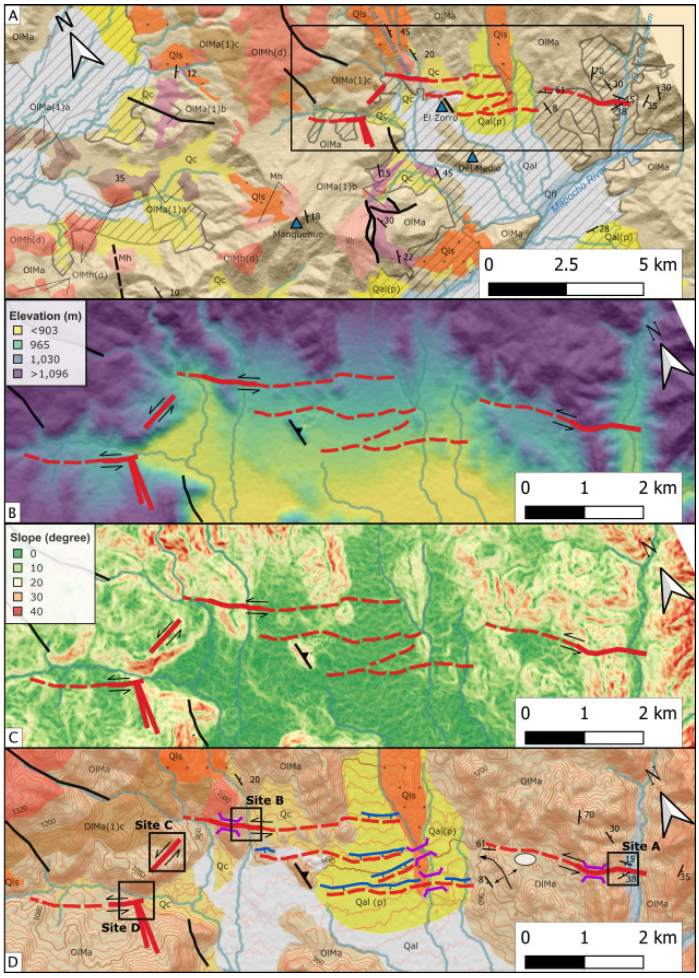

FIG. 2. **A.** Simplified geological map of study area. The map shows topography, lithology, Quaternary deposits, major structures and hydrology, and "island hills" (in blue triangles). Black box shows the locations of figure 2B-C-D. **Qal**: Quaternary alluvial deposits; **Qfl**: Quaternary Maipo River fluvial deposits; **Qal(p)**: Quaternary alluvial piedemont-deposit; **Qls**: Quaternary landslides; **Qc**: Quaternary colluvial deposits; **Mh**: Subvolcanic andsites and dacites; **OlMa**: Oligo-Miocene Abanico Formation constituted by andesitic to basaltic lavas interbedded by tuffs and continental sedimentary rocks; **OlMa1(a)**: Dacitic to rhyolitic to welded tuffs; **OlMa1(b)**: Sedimentary intercalation of fluvial conglomerates, sandstones and shales; **OlMa1(c)**: Acid cineritic tuffs; **OlMh(d)**: Stocks of basaltic andesites to dacites; hatched area are urban zones. Major faults identified by other authors are shown with thick black lines. EAF trace is shown in thick red lines, arrows shows kinematics. Hydrology is shown in light-blue lines. Geology compiled from Thiele (1980), Wall *et al*. (1999) and this work. **B.** DEM of the study area coloured by elevation. The EAF is indicated. **C.** Slope map of the study area with the EAF. **D.** Quaternary geological map of the study area and with specific study sites (A-D) shown (black boxes). Scarp are shown by hick blue lines, with the down-thrown block indicated. White ellipse shows sag pond location. Purple lines indicate the location and orientation of saddles.

La Dehesa basin. Given that these sites are heavily urbanized (Fig. 2A) and crossed by roads, modern Quaternary mapping is challenging due to severe human and construction-induced modifications. Furthermore, as most of the area is private property (in most cases walled off) the access is not always possible. Fault rocks were classified following Sibson (1977). A combination of remote sensing and field mapping was used to explore tectonic geomorphology and landforms such as deflected streams, saddles, sag ponds and scarps (McGill and Sieh, 1991; Burbank and Anderson, 2012) in order to determine the evidence fault surface expression (Fig. 2B-D).

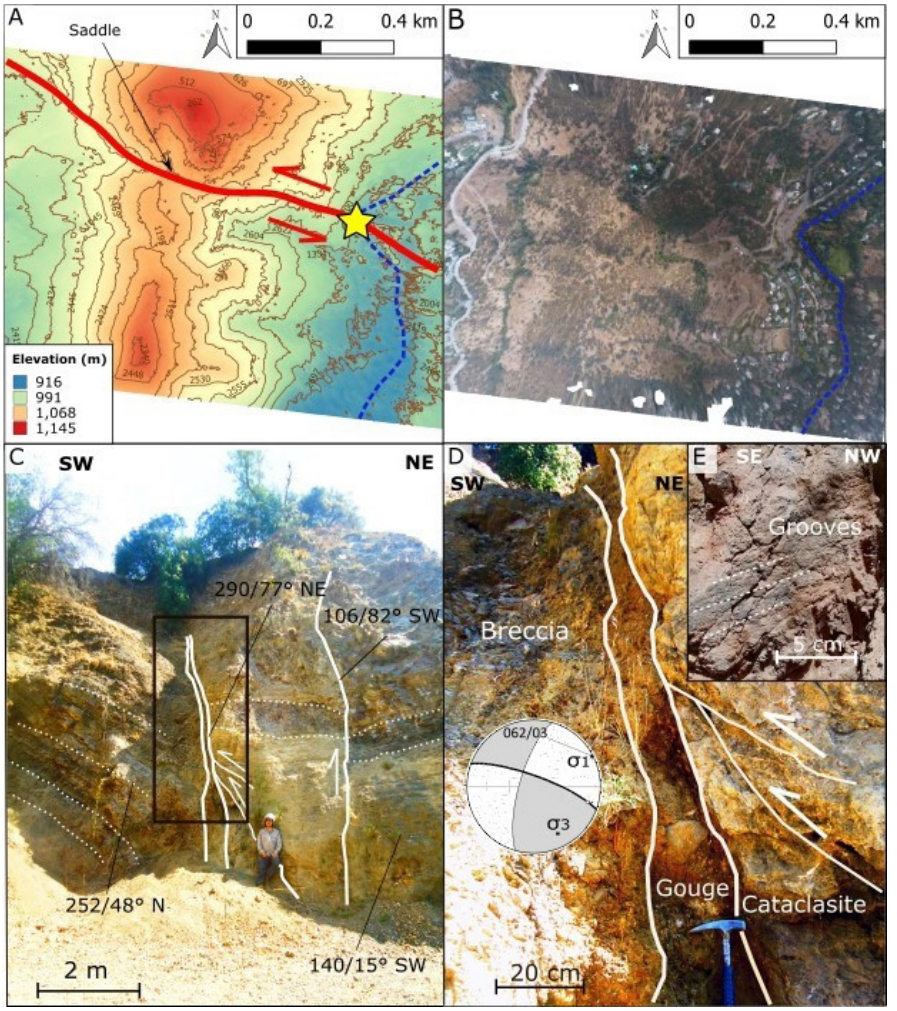

FIG. 3. **A.** SfM DEM from Site A. Yellow star shows the location of the fault outcrop in figure 3C. Dotted blue line shows the El Arrayán stream. Red line shows the approximate location and kinematics of the EAF. **B.** Orthophoto derived from SfM. Dotted blue line shows the El Arrayán stream. **C.** Field photo of EAF at Site A in El Arrayán. Black inset shows the location of figure 3D. **D.** Field photographs of fault rocks within the EAF fault core. Stereonet shows sigma 1. Note minor reverse fault in cataclasite. **E.** Grooves on SW main slip plane.

Digital topographic data was obtained from two sources. Open-access digital elevation models (DEM) from ALOS (Land Observing Satellite) PALSAR (Phased Array type L-band Synthetic Aperture Radar), that covers the entire Santiago Metropolitan area, and DEMs derived from drone photographs, generated by photogrammetric techniques. The ALOS PALSAR DEM provides open-access 12 m resolution radiometric terrain corrected DEMs in GeoTIFF formats, which were used for mapping and spatial analysis in QGIS software. Site specific DEMs along the EAF were constructed with Structural from Motion (SfM) techniques (Förstner and Pertl, 1986; Harris and Stephens, 1988). SfM is a photogrammetry technique that allows the reconstruction of a three-dimensional (3D) scene from a series of two-dimensional (2D) images. The 3D visual models and DEMs were created with photographs collected with a Phantom 4 (DJI) drone (UAV) using the Argisoft 1.3.2 software to create DEMs and digital orthophotos.

The kinematic analysis, based on field observations, was performed with FaultKinTM software (Marret and Allmendinger, 1990; Allmendinger *et al*., 2012). This software uses the right dihedral geometrical

method of Angelier and Mechler (1977) and Pfiffner and Burkhard (1987) for calculating the orientation of the compressional and tensional axes of individual fault planes and fault populations based on structural data.

Finally, the seismic hazard of the EAF was explored based on the distribution of fault rocks and geomorphological mapping evidence, which was evaluated using Wells and Coppersmith (1994) fault parameter scaling laws.

3. Results

3.1. Geologic fault observations

The discovery of the EAF in El Arrayán lead us to work, map and conduct further field investigations to the west of El Arrayán. Field mapping in Lo Barnechea area shows volcanic and sedimentary rocks of the Abanico Formation (Fig. 2A-D). The strike and dip of the bedding in the Abanico Formation in this area differs significantly from the rest of the mountain front, especially in the San Ramón Range and eastern side of the El Arrayán Valley, where it primarily dips east (*e.g.*, Riesner *et al.*, 2017). This could be due to the influence of the EAF which crosscuts the stratification and post depositional folding in the Abanico Formation and represents the youngest deformation observed within this formation.

3.1.1. Main fault exposures

The main fault exposure is located in the El Arrayán neighbourhood, adjacent to the El Arrayán stream, a tributary to the Mapocho River in Lo Barnechea, within northeastern Santiago (Fig. 2D, Site A). The road cut on the west side of the "Camino Refugios del Arrayán" (between turn off to Camino el Estero and Camino Mallalil), exposes stratified andesites interbedded with dark-coloured fine-grained sedimentary rocks (siltstone/mudstone, 1-5 cm thick: Fig. 3C). The exposure is ~15 m high and ~30 m long. Dark-grey fine-grained siltstone/mudstone beds are inclined (250-270/38-50° N) to the left (south) and they are in faulted contact with relatively flat-lying (140/10-20° SW) volcanic and sedimentary layers to the north. Within the fault zone itself, a series of fault rocks were found (Fig. 3C-D).

The fault rocks constitute the core of the EAF (*e.g.,* Caine *et al*., 1996). The fault core is a 3.5 to 4.0 m wide fault sequence with crush breccia, protocataclasites and fault gouge layers (Fig. 3D, Sibson, 1977). The principal slip zone is characterized by gouge and the two sub-vertical gouge-lined planes (290/77°NE: Fig. 3C-D). Sub-horizontal fault grooves (*i.e.*, slickenlines) along the two main slip planes shows slightly dipping rakes between 12-8°E, indicating mainly strike-slip kinematics (Fig. 3E). Unfortunately, no sense of movement could be determined *in situ*, however a left-lateral deflection of the El Arrayán Creek immediately adjacent to the site suggests a sinistral kinematics (Fig. 3A-B). According to the rake angle and left-lateral kinematics (Marret and Allmendinger's, 1990 methodology), the fault likely accommodates mostly strike-slip motion with minor north oriented dip-slip (up to the north) and sigma 1 of 062/03° (Fig. 3D). A subsidiary slip plane (106/82° S) displaces a brown volcanic lava bed, with a 1 m vertical throw (Fig. 3C). Altogether, with the northern main slip plane they form a light-colored wedge shaped block of protocataclasite with abundant gypsum veins (Fig. 3C). The protocataclasite is curved, concave and close to the main slip zone (Fig. 3D), in a similar way to drag folds in discrete reverse faults. The protocataclasite is also faulted with centimeter-scale displacements along by minor NE dipping reverse fault planes (Fig. 3D).

In addition to the EAF exposures in El Arrayán, geomorphic mapping and field reconnaissance (see below) allowed the recognition of a second EAF exposure in western Lo Barnechea, where the Juan Pablo II road connects Lo Barnechea with Chicureo, ~11 km to the west of Site A (Fig. 2D, Site D; in a road cut along the southern side of Juan Pablo II Road). In this locality massive porphiric dark red andesites from the Abanico Formation to the north are juxtaposed and fault contact with massive porphyric light-grey andesites to the south. Between both rock units is a 70 m-wide highly sheared fault zone. Numerous meter-wide fault rock panels, including breccias and protocataclasites were found (Fig. 4A-D), as well as sub vertical sharp individual fault planes in variable orientations (Fig. 4B). Along the NW side of the fault zone the most prominent structure (*i.e.*, the master fault) was observed. This is a ~1.5 m wide, white coloured, S-shape protocataclasite with numerous minor faults planes with S-C fabric and gypsum veins, which suggest reverse kinematics (Fig. 4A). Flanking the S-shape protocataclasite to the NW, there are sub-horizontal (5-15°) slickensides with left-lateral kinematics in a 110/83° SW orientated fault

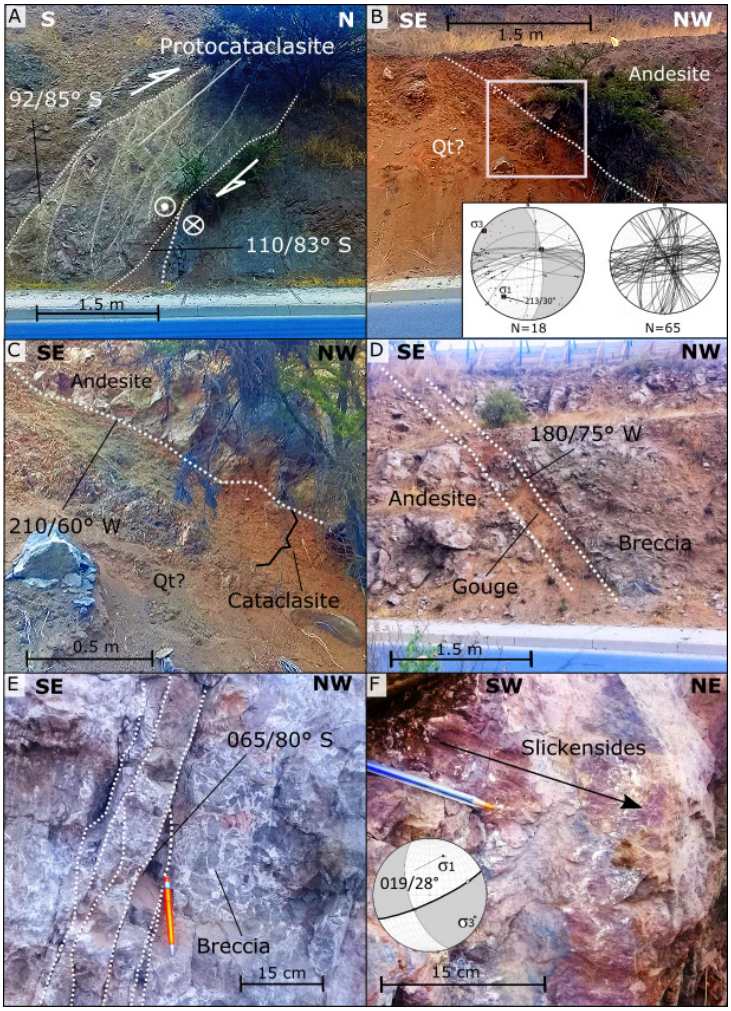

FIG. 4. **A.** Field photo of EAF outcrop with WNW-ESE orientation at Site D. Dotted white line shows fault surfaces. **B.** Field photo of the EAF minor ~N-S fault at Site D. White box shows the location of figure 4C. Stereonets show the structural data obtained in Site D. **C.** Close view of the fault outcrop shown in figure 4B. **D.** Field photo of the EAF minor N-S fault at Site D. **E.** Field photo of the EAF ENE-WSW minor fault at Site C. **F.** Field photo showing subhorizontal slickenlines and grooves at Site C. Stereo net shows sigma 1 obtained in Site C.

plane. This fault plane has very similar orientation as the main fault planes (106/82° SW) described at Site A. The width of the fault zone allowed the measurement of 65 individual fault planes, veins and fractures, 18 of them with likely kinematic indicators (Fig. 4B). Based on field data, a mean sigma 1 of 213/30° (Fig. 4B) was determined for that fault population (Marret and Allmendinger, 1990; Allmendinger *et al*., 2012). A W-E structural trend with left-lateral strike-slip kinematics is clearly visible in the stereonet plot (Fig. 4B). A 210/60° W orientated, 10-30 cm wide, protocataclasite juxtaposes volcanic dark-reddish massive andesite in the hangingwall with presumably Quaternary materials (Fig. 4C). Specifically a poorly-consolidated, orange silt to fine grain sand matrix with semi-rounded volcanic fragments (50 to 1 cm across) and no clear sedimentary structures. Additionally, an 185/40° W orientated, ~10-30 cm wide protocataclasite, juxtaposes the alluvium in the hangingwall with a ~7 m wide fault breccia in the footwall. Finally, the fault breccia is bounded to the SW by a 180/75° W fault plane, juxtaposing it against a massive light-grey andesite (Fig. 4D).

Two other fault sites were found in this highly urbanised zone (Fig. 2D, Site B and C). Site B is a 6 m wide fault zone in between massive porphyric andesites (Fig. 5A-B; yellow star). In this location the cataclasite, breccia and gouge have a W-E to WNW-ESE strike with sub-vertical dips to the north (Fig. 5C). In spite no kinematics indicators being found, the possible left-lateral stream deflection in Las Hualtatas stream (immediately adjacent to the site), suggests sinistral kinematics (Fig. 5A-B). A NW-oriented saddle is found to the West of the fault (Fig. 5A). To the West of the saddle, at the Santa Martina road, another fault zone is found (Fig. 5A; orange star). This fault is formed by massive purple and grey andesites that are cut by 3 subvertical 5-30 cm wide fault rocks (breccia and cataclasite) and associated fault planes (Fig. 5D). These fault planes vary from 330 to 350° with no kinematic indicators. At Site C, grey aphanitic volcanic rocks with sub-horizontal fractures have a 4 m-wide deformation zone. It is characterized by 6 subvertical minor fault planes with subhorizontal grooves with a dextral sense of motion with a mean 065° strike. A 10-20 cm wide fault breccia was observed immediately adjacent

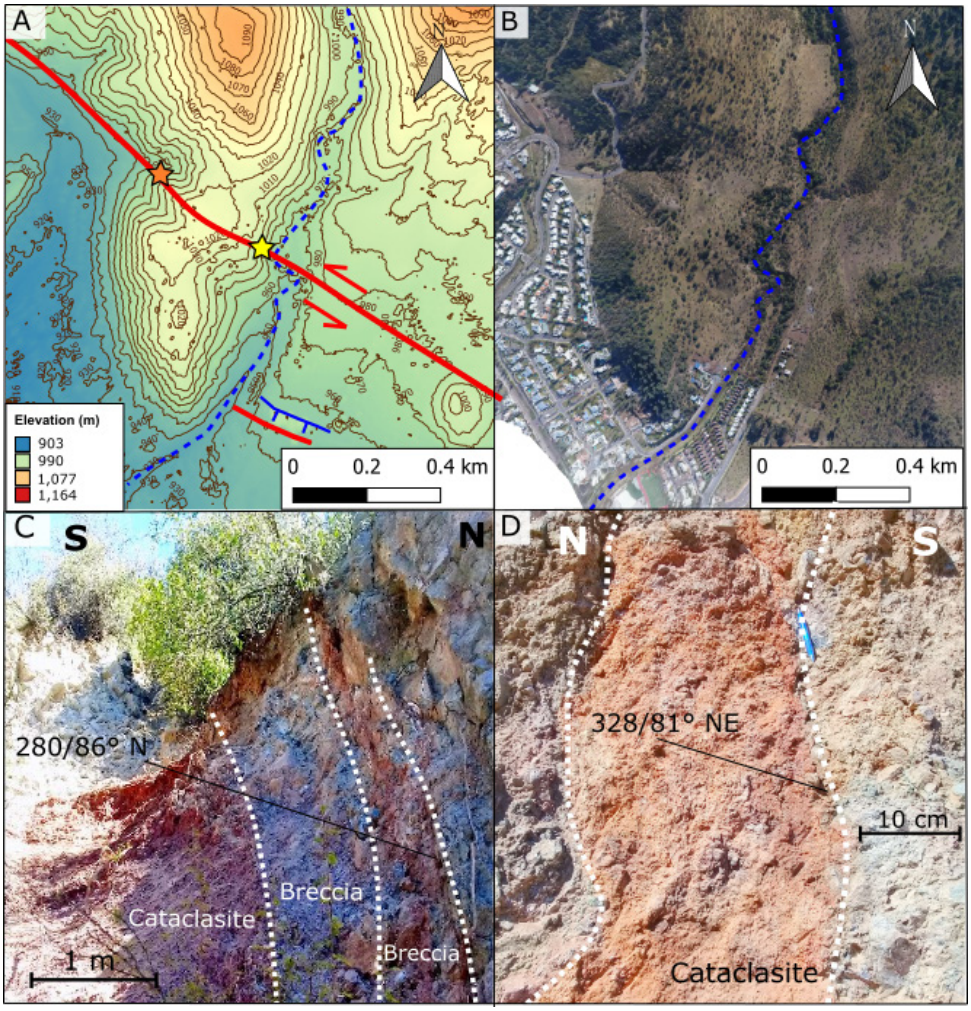

FIG. 5. **A.** SfM DEM from Site B. Yellow star shows the location of fault outcrop of figure 5C. Orange star shows the location of fault outcrop of figure 5D. Red lines shows the aproximate location and kinematics of the EAF. Dotted blue line shows the location of the Hualtatas stream. Solid blue line represents a fault scarp with the down-thrown block indicated. **B.** Orthophoto derived from SfM of Site B. Dotted blue line shows location of the Hualtatas stream. **C.** Field photo of the EAF in the Hualtatas stream at Site B. **D.** Field photo of the EAF at "Santa Martina" road in Site B.

to a 065/80° SE fault plane (Fig. 4E) with a 30° rake groove with Riedel fractures that indicates a left-lateral strike-slip kinematics (Fig. 4F). The fault plane and grooves data allowed us to obtain a mean compression sigma 1 of 019/28° (Fig. 4F; after Marret and Allmendinger, 1990; Allmendinger *et al*., 2012).

Additionally, a NW-plunging anticline was recognized within the study area (Fig. 2D). This anticline has similar orientation with a NW orientated hill (Fig. 2B-C) suggesting structural control.

3.2. Remote sensing and geomorphic observations

Within the study area, in Lo Barnechea, there are conspicuous low areas with respect to the surrounding elevations, within the foothills of the Principal Cordillera, north of the Mapocho River and east of the Manquehue Hill (Fig. 2A). These low areas were infilled by Quaternary sediments from the Mapocho River and with piedmont Quaternary alluvial and colluvial material derived from the surrounding hills (Fig. 2A). Urban development is concentrated in these low-lying areas (*e.g*., La Dehesa) at an average elevation of 850 m (Fig. 2B). Quaternary alluvium deposits with fan morphologies are well exposed (Fig. 2D), draining from NNE to SSW (Fig. 2B-C). Isolated hills (almost island hills) disrupt the average south-west facing 3-4° slopes (Fig. 2C) reaching elevation up to 970 m in the Medio and El Zorro Hills which have a NNW to NW elongation, and are composed of sedimentary Abanico Formation rocks (Fig. 2A). North of El Zorro Hill, three en-echelon left-stepping NNW-elongated hills are aligned in a WNW-ESE orientation (Fig. 2B-D). The eastern limit of the La Dehesa depression has an irregular morphology composed by numerous hills, some with a WNW to NW elongation (Fig. 2B-C). Quaternary mass wasting (*i.e*., landslide) deposits were found within this area, which exhibits long and narrow N-S to NNE-SSW orientated shapes with numerous saddles along them (Fig. 2D).

Slope maps (Fig. 2C) combined with topographic profiles (Fig. 6A), demonstrate the presence of aligned discontinuous, tectonic landforms, such as sag ponds, drainage pattern perturbations, saddles and topographic steps or breaks in the slopes of these fans (~10-14° and between 3-14 m in elevation). These topographic steps are semi-parallel, with crests that strike E-W to NW-SE (Fig. 2D) that contrast with the NNE to SSW drainage pattern (Fig. 2C). The topographic steps coincide with the island hills that disrupt the low-lying basin around the La Dehesa area.

At Site A, a left-lateral displacement of the El Arrayán stream (immediately to the east of the fault outcrop) suggests left-lateral strike-slip kinematics for the EAF (Fig. 3A-B). However, landslides or slope deposits from the valley side to the East may be responsible for an apparent deflection. A NW-oriented saddle in the main ridge between El Arrayán and La Dehesa (site A, Fig. 3A) immediately to the west and along strike from the fault exposure (Site A) is noteworthy (Fig. 3A). This ridge has higher elevations to the north on the hangingwall of the fault, which is suggestive of long-term up to the north dip slip motion in addition to the dominant strike-slip motion there (Fig. 3A). Further to the west, aligned with the saddle and the fault zone, a possible sag pond *(i.e.,* the Lo Barnechea lagoon) is exposed in a relative flat area between irregular hills (Fig. 2D).

Geomorphic evidence and topographic scarps indicate the presence of fault strands of the EAF between Sites A and B, in the Quaternary alluvium within the La Dehesa depression (Fig. 2D). The southern strand is inferred by a ~150 m long, WNW-ESE oriented, SSW-facing scarp of ~12 m high and ~12° dip between surfaces (Fig. 6 A, P5). This scarp is aligned with a saddle on irregular Quaternary alluvial deposits (Fig. 2D). West of the saddle, a ~1.5 km long WNW-ESE orientated scarp was recognized on a Quaternary alluvial deposit with an average ~10° dip and is ~9 m high in its central part (Fig. 6 A, P4). This semi continuous scarp and saddle alignment suggest the presence of a WNW-ESE fault with up to the north sense of motion (*i.e*., coincident with observations from Site A). Unfortunately, no in-situ structural data is available in order to validate the geomorphological observations. Further north, the next strand is inferred by the presence of a ~600 m length, WNW-ESE oriented, SSW-facing topographic scarp which is ~11 m high and has a 14° dip between surfaces along the Quaternary alluvial deposit (Fig. 6 A, P3). The western part of the strand is ~200 m long, WNW-ESE, SSW-facing topographic scarp of ~3 m and with a ~12° dip found in Quaternary colluvial deposits (Fig. 6 A, P1). Between both of the aforementioned scarps, the continuity of the strand is associated with three en-echelon left-stepping NNW-elongated hills aligned in a WNW-ESE orientation (Fig. 2B-C-D). These landforms commonly appear

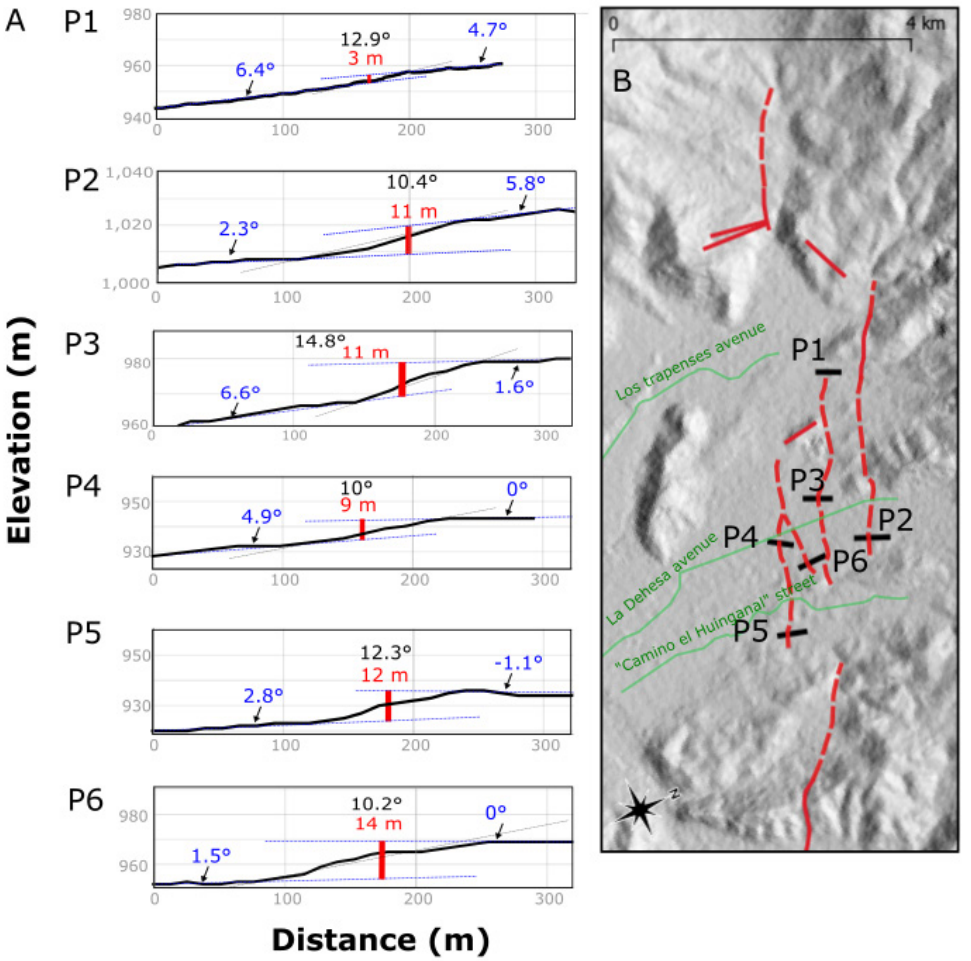

FIG. 6. **A.** Topographic profiles of the study area. P1 extracted from SfM DEM. P2-P6 extracted from ALOS-PALSAR DEM. **B.** Location of topographic profiles of the study area. Solid red lines shows locations of observed EAF traces, dashed red lines show the locations of inferred EAF strand. Green lines show the main roads of the study area within the La Dehesa area of Lo Barnechea.

between parallel left-lateral right stepping strike-slip faults (Wilcox *et al.,* 1973; Sylvester, 1988 and references therein). A retrospective analysis of the 2019 Ridgecrest California Mw 6.4 earthquake (which involved two different faults), demonstrated that the sinistral strike slip and ~17 km-long rupture (along a previously unknown fault) had subtle geomorphic evidence of previous surface ruptures with scarps, deflected drainages, aligned hills (Thompson Jobe *et al.,* 2020), very similar with what is observed along the EAF. Unfortunately, no *in situ* structural data became available to confirm the geomorphological observations and to constrain the geometry and kinematics of the inferred fault strand. The aligned morpohotectonic features that connect the two key fault exposures in the east and west, allows inference of the presence of a WNW-ESE left-lateral strike-slip fault with minor uplift along the northern side of the fault. Between both strands, a W-E trending scarp is found (Fig. 6A, P6). This scarp is ~0.7 km in length, faces to the south, dips 10° and is ~14 m high. To the east, this scarp is aligned with a prominent saddle in between a Quaternary landslide (Fig. 2D). The presence of this scarp allows the inference of a W-E striking fault. The northern strand between Sites A and B is inferred by a WNW-ESE oriented, ~600 m length, SSW-facing scarp of ~11 m high and 10° dip in Quaternary alluvial deposit (Fig. 6A, P2).

The strand is aligned to the west with the northern termination of the three NNW-elongated hills, and with a displaced stream adjacent to the fault outcrop at Site B (Fig. 2B-C).

At the westernmost portion of the study area, a WNW-ESE linear valley suggest that this fault zone continues from Site D to the west (Fig. 2B-C), making it at least 13 km long. The road coincides with the strike of the fault zone. The road associated urbanization and private property impedes the collection of additional field data necessary to define the EAF's western extension.

4. Discussion

4.1. Geometry and kinematics

The internal architecture of the EAF is characterized by a network of semicontinuous subparallel and oblique faults (Fig. 2). This semi continuous assemblage is compatible with strike-slip fault system geometry (Naylor *et al.,* 1986; Woodcock and Fischer, 1986; Sylvester, 1988). The intense urbanization (Fig. 2A) and access to private property limited data collection, possibly hiding important structural and geomorphic data and the possibility of further analysis. The EAF orientation and kinematics are in agreement with the internal structure of the Abanico Basin proposed by Piquer *et al.* (2016) being part of the NW-striking strike-slip fault system.

The main strike-slip kinematics of the EAF is clear in the morphology (Fig. 2D) and in the *in situ* structural data. However vertical motion is evident along some of the EAF main segments as oblique grooves at site A and D (Figs. 3E and 4F), discrete reverse fault planes (Fig. 3C), and fault scarps with the north side up (Fig. 2D), which is consistent with the higher-to-the-north EAF topography. This suggests that WNW-ESE main segments of the EAF not only accommodate strike-slip faulting, but also N-S shortening. Therefore, the stress regime of the EAF is transpressional (*i.e.,* sinistral-reverse -up to the north). The only evidence of normal faulting are minor faults reported in Site D with orientations varying from WNW-ESE to ENE-WSW (Fig. 4B). This normal fault component can be attributed to local extension along previously formed joints proximal to main EAF strands. An alternative explanation for this normal component is that some of the faults are closely parallel to the ENE-WSW principal stress direction, and may be accommodating part of the local extension in the strike slip fault system or a stepover connecting to an eastern continuation of the EAF coincident with the Mapocho River.

4.2. Potential for Quaternary activity

Through cautious reflection regarding of all of this evidence, it important to consider if the EAF is an active structure that may cause earthquakes and surface rupture hazards from faulting within northeastern Santiago.

We have documented for the first time a >13 km long young fault system (*i.e.,* the EAF) that formed within urban Santiago. These faults cut the NS trending folded stratigraphy of the Abanico Formation and developed long after the folding formed. Based on geomorphological evidence Late-Quaternary activity is inferred.

The Abanico Formation rocks deposition perhaps occurred between the Oligocene and Miocene (~34 to 5 Ma; Charrier *et al.*, 2002, 2007; Giambiagi *et al.*, 2003; Fock, 2005). However, new dating and fieldwork (Mosolf *et al*., 2019) from southeast of Santiago (~35° S) provides a robust and much older chronostratigraphic framework spanning *ca*. 75-11 Ma. Thus if the Abanico basin is much older than previously recognized, where the Late-Cretaceous to Late Eocene intra-arc sedimentation and volcanism were followed by Late Eocene to Late Miocene strike-slip dextral shearing within the volcanic arc, it implies that the strike slip faulting could have commenced during the Eocene. If that is the case, then the EAF could correspond to older exhumed faults and not to active Quaternary ones. However, recent work on the internal conjugate strike-slip fault systems within the Abanico Formation (Piquer *et al*., 2017) show a Middle Miocene-Early Pliocene activity. Based on current seismicity and the distribution of active volcanic centres, Piquer *et al*. (2019) further suggest that some of these faults are still active under the current stress regime. Present day ENE-WSW (N77°-78°E) plate tectonic convergence direction (DeMets *et al*., 1994; Gripp and Gordon, 2002) and the GPS ENE-WSW (N72°E) velocity field directions (Brooks *et al*., 2003) are consistent with the ENE-WSW (Az 65°) principal stress direction inferred for the EAF. This analysis is well supported by the principal stress orientation ($\sigma 1$) obtained

from fault plane kinematic analysis. The variations in the σ1 orientations can be attributed to local stress reorientations, which can differ from the main structures. On the other hand, regional stress inversions (Pérez *et al.*, 2014) along the San Ramón Fault and seismicity analysis (Ammirati *et al*., 2019) along the western flank of the Andes, suggests that the seismicity is accommodating NE-SW compression, and thus also consistent with our EAF results. This indicates that the EAF orientation and kinematics are compatible with the modern ongoing first-order neotectonics. Therefore, the seismicity and regional stresses support the current activity along the EAF, however the lack of local dates of the rocks around the EAF leads to ambiguous results regarding long-term Late-Cenozoic activity.

However, the geomorphology along the EAF provides evidence for Quaternary activity, as the EAF cross-cuts the Quaternary landforms composed of bedrock (*e.g.*, the ridge between El Arrayán and La Dehesa) and Late-Quaternary deposits, for example those in the La Dehesa area. Neotectonic lineaments, inflection points and likely strike slip fault scarps in Late-Quaternary fans, deflected streams, displacements of the main ridge between El Arrayán and La Dehesa, pop up "island hills" in the La Dehesa basin coincident with bedrock exposures of the EAF provides strong evidence for Late-Quaternary activity. The highly urbanized nature of La Dehesa creates challenges for data acquisition as well as for establishing the connectivity of structures. This limitation however shows the strength of the tectonic geomorphology of the EAF, as it can be seen in spite of crossing a highly urbanized area. The occurrence of large landslides on the hanging wall of the EAF constitutes additional support of fault activity, as landslides tend to occur on the hangingwall of faults with a vertical component (Fig. 1B; *e.g.*, Serey *et al*., 2020). Therefore in the absence of absolute dates, the tectonic geomorphology constitutes important chronological support.

Other Quaternary faults reported in the Andes of Central Chile are the SRF (Rauld, 2002; Armijo *et al*., 2010; Rauld, 2011) and the San José de Maipo Fault (Lavenu and Cembrano, 2008). Due to the N-S to NNW-SSE orientation and present day reverse kinematics of the SRF, an E-W to ENE-WSW principal stress orientation is attributed to the SRF (Rauld, 2011). The principal stress direction on the SRF is similar and compatible with that of the EAF stress direction, and with modern ongoing first-order tectonic compressional settings (Ammirati *et al*., 2019). Lavenu and Cembrano (2008) proposed a NNW-SSE oriented principal stress for the San José de Maipo Fault. This fault is only locally visible at one exposure with no geomorphic fault traces, this suggests it may correspond to a small-scale structure that accommodates local stresses. Implicit in the argument is that the derived principal stresses along the San José de Maipo Fault may not represent the regional scale principal stress orientations (*i.e.*, SW-NE; Ammirati *et al*., 2019), nor have similar earthquake and fault rupture hazards as the SRF and the EAF that exhibit several km along strike with a clear geomorphologic expression.

The seismic sequence that occurred in July 2019 near Ridgecrest, California provides insights regarding the potential activity of the EAF. Two fault ruptures occurred in this sequence with Mw 6.4 and Mw 7.1 earthquakes, respectively (Thompson Jobe *et al*., 2020). The sinistral rupture of the Salt Wells Valley fault zone (SWVFZ) during the Mw 6.4 event was ~21 km long, and occurred along a largely unidentified fault, in which only 37% of the fault zone was mapped prior to the Ridgecrest earthquakes (Thompson Jobe *et al*., 2020). However, post-event mapping of pre-2019 imagery allowed Thompson Jobe *et al*. (2020) to establish that at least 59% of the length of the fault had pre-existing tectonic geomorphology features (*e.g.*, scarps, deflected drainages, lineaments, and contrasts in topography or vegetation and ground colour) that coincident with the fault that subsequently ruptured in 2019. These authors state that in the pre-rupture imagery, of the fault-related features, only 53% were relatively "obvious", while 7% was "subtle". One of the authors of this paper (De Pascale) participated in post-earthquake reconnaissance along the Mw 6.4 Ridgecrest rupture and fault mapping. He became struck by the low-lying hills that pop-up out of the South Californian flat landscape along the fault and the striking similarity with the La Dehesa hills along the EAF. Since over a 60% of the along-strike trace of the EAF (between sites A and B, about 14 km) have been mapped, showing similar neotectonic scarps, deflected streams and lineaments, as those reported from along the Ridgecrest earthquake Mw 6.4 rupture, therefore the features along the EAF suggest they were generated from Late-Quaternary EAF fault ruptures.

4.3. Tectonic implications

At a regional scale, the western flank of the Andes in Central Chile are characterized by the presence of the WATS (Armijo *et al*., 2010). The SRF is the most prominent expression of the WATS (Armijo *et al*., 2010; Rauld, 2011; Pérez *et al*., 2014; Vargas *et al*., 2014; Estay *et al*., 2016; Riesner *et al*., 2017), although its continuity to the north and south is not well established (Armijo *et al*., 2010; Estay *et al*., 2016; Riesner *et al*., 2017). The location, orientation, kinematics and recent Quaternary activity, allows the suggestion that the EAF corresponds to a transfer system that links the WATS fault and the SRF to the west with other N-S striking reverse faults part of the WATS system. The abrupt morphological changes of the Principal Cordillera to the north of the Mapocho River, and the near-surface complexity along the northern portion of the SRF, suggests a westward deformation transfer by the EAF towards the Central Depression, as shown by a gentle NW striking anticline placed along a group of three arch-shaped "island" hills, is consistent with the hypothesis of deformation being transferred.

4.4. Potential EAF seismic hazard

Given that the EAF is an active Quaternary crustal structure that fails with stick-slip behaviour, as suggested from the tectonic geomorphology, a surface rupture of 13 or more km within a 15 km thick seismogenic upper crust, as supported by upper crustal microseismicity (Ammirati *et al*., 2019), suggests a seismic potential of at least Mw 6.4 (using the earthquake scaling relations of Wells and Coppersmith, 1994). Should the fault length be longer or the seismogenic zone thicker than as reported by Ammirati *et al*. (2019) the Mw 6.4 would be an under-estimate. Just for comparison purposes the February 2011 Mw 6.3 earthquake along the blind (*i.e.*, non-surface rupturing) Port Hills fault (Li *et al*., 2014), was responsible for NZ$30 billion in damage to the City of Christchurch in New Zealand. In fact, ruptures along strike slip faults to the surface are not common below Mw ~6.0 (*e.g*., Schwartz, 2018), thus having strong tectonic geomorphology from previous fault ruptures in the Quaternary suggests that earthquakes of this magnitude have occurred along EAF previously. Clearly, if only portions of the EAF ruptured instead of the entire section between sites A and B, this event would be <Mw 6.4. If the EAF ruptures in conjunction with the SRF, something that the recent Kaikoura earthquakes in New Zealand demonstrated is a possibility (*i.e.*, ruptures that continue along interconnected active structures) with correspondingly larger energy release than through individual fault ruptures alone, then the pre-existing estimates for seismic hazard along the SRF (Mw 7.5 *e.g.*, Vargas *et al*., 2014) may be an underestimate.

5. Conclusions

Remote sensing and fieldwork allowed the discovery, characterization and mapping of the unreported El Arrayán fault (EAF), in northeastern urban Santiago. The fault has upper crustal fault rocks (*e.g.*, Sibson, 1977) including gouge, cataclasite, and breccia and cuts the folded Abanico Formation stratigraphy. This documents for the first time fault rocks at the surface within the City of Santiago. The EAF is a subvertical WNW-ESE structure with strike-slip left-lateral kinematics. The EAF has semicontinuous fault strands (which may be only discontinuous due to urban development) in addition to minor strike-slip and reverse faults. The EAF location from exposures and strike coincide and are aligned with deflected streams, a displaced ridgecrest (between El Arrayán and La Dehesa), fault scarps, lineaments, a sag pond and a linear valley, which are all evidence of Late-Quaternary tectonic geomorphology. The present day ENE-WSW plate tectonic convergence direction (DeMets *et al*., 1994; Gripp and Gordon, 2002) and the ENE-WSW GPS velocity field directions (Brooks *et al*., 2003) are consistent with the orientation of σ1 derived from the kinematic analysis with fault slip planes and the ENE-WSW (065°) principal stress direction inferred for the EAF based on sigma 1.

The occurrence of large landslides along the hanging wall of the fault provides additional supporting evidence for activity. The geomorphic evidence coincides with well-exposed fault traces and fault rocks located along and cross-cutting the Abanico Formation and Quaternary sediments. This configuration supports the interpretation that the EAF is a likely a Quaternary structure that accommodates upper crust tectonic deformation, and as such has a surface rupture potential and seismic hazard of at least up to Mw 6.4, that could increase if the EAF

connects with the SRF. We suggest that further work is required to determine the last EAF rupture age. These works should include fault trenching, geophysics and Quaternary dating aimed at a better definition how these faults interrelate. Needless to say, the presence of an important crustal fault within a highly populated and quickly urbanizing part of Santiago constitutes a potential risk, particularly given the lack of fault rupture avoidance-surveys and legislation.

Acknowledgments

This study was funded by NERC-Newton Fund grant NE/N000315/1. Postgraduate students M. Pérsico, F. Sandoval, S. Perroud, M. Hernández, S. Pairoa of the neotectonic group of U. Chile provided useful comments, observations, and assistance in the field. De Pascale is also supported by a Fondecyt Grant #11160038 by ANID/CONICYT to work on active faults. Thanks to the other Newton Fund researchers for valuable discussions and insights in the field regarding this topic including D. Petley, M. Froude, W. Murphy, and M. Brain. Portions of this work were part of the MSc work by Araya, and the Honour Thesis by Mardel in the Department of Geology at U. Chile. Thanks for feedback from G. Easton, L. Pinto, and S. Rebolledo on aspects of the neotectonics of Santiago, WATS, and the SRF. Tremendous thanks to J. Skarmeta for thoughtful reviews and suggestions that improved our paper and thanks to the Editor of Andean Geology (W. Vivallo) for reviewing this work and for expert feedback as well. This is the Universidad de Chile's Neotectonic group contribution #47.

References

Angelier, J.T.; Mechler, P. 1977. Sur une méthode graphique de recherche des contraintes principales également utilisables en tectonique et en séismologie: la méthode des dièdres droits. Bulletin de la Société Géologique de France 7 (6): 1309-1318.

Allmendinger, R.W.; Cardozo, N.; Fisher, D.M. 2012. Structural geology algorithms: Vectors and tensors. Cambridge University Press: 286 p. Cambridge.

Alvarado, P.; Barrientos, S.; Sáez, M.; Astroza, M.; Beck, S. 2009. Source study and tectonic implications of the historic 1958 Las Melosas crustal earthquake, Chile, compared to earthquake damage. Physics of the Earth and Planetary Interiors 175 (1-2): 26-36.

Ammirati, J.B.; Vargas, G.; Rebolledo, S.; Abrahami, R.; Potin, B.; Leyton, F.; Ruiz, S. 2019. The Crustal Seismicity of the Western Andean Thrust (Central Chile, 33°-34° S): Implications for Regional Tectonics and Seismic Hazard in the Santiago Area. Bulletin of the Seismological Society of America 109 (5): 1985-1999.

Armijo, R.; Rauld, R.; Thiele, R.; Vargas, G.; Campos, J.; Lacassin, R.; Kausel, E. 2010. The West Andean thrust, the San Ramón fault, and the seismic hazard for Santiago, Chile. Tectonics 29 (2): 1-34.

Barrientos, S.; Vera, E.; Alvarado, P.; Monfret, T. 2004. Crustal seismicity in central Chile. Journal of South American Earth Sciences 16 (8): 759-768.

Brooks, B.A.; Bevis, M.; Smalley Jr, R.; Kendrick, E.; Manceda, R.; Lauría, E.; Maturana, R.; Araujo, M. 2003. Crustal motion in the Southern Andes (26°-36° S): Do the Andes behave like a microplate? Geochemistry, Geophysics, Geosystems 4 (10), 1085: 1-14.

Burbank, D.W.; Anderson, R.S. 2012. Tectonic Geomorphology, 2nd edition. Blackwell Publishing Ltd.: 454 p. Oxford.

Candia, G.; De Pascale, G.P.; Montalva, G.; Ledezma, C. 2017. Geotechnical aspects of the 2015 Mw 8.3 Illapel megathrust earthquake sequence in Chile. Earthquake Spectra 33 (2): 709-728.

Caine, J.S.; Evans, J.P.; Forster, C.B. 1996. Fault zone architecture and permeability structure. Geology 24 (11): 1025-1028.

Charrier, R.; Wyss, A.; Flynn, J.J.; Swisher III, C.C.; Norell, M.A.; Zapatta; F.; Novacek, M.J. 1996. New evidence for late Mesozoic-early Cenozoic evolution of the Chilean Andes in the upper Tinguiririca valley (35° S), central Chile. Journal of South American Earth Sciences 9 (5-6): 393-422.

Charrier, R.; Baeza, O.; Elgueta, S.; Flynn, J.J.; Gans, P.; Kay, S.M.; Muñoz, N; Wyss, A.R.; Zurita, E. 2002. Evidence for Cenozoic extensional basin development and tectonic inversion south of the flat-slab segment, southern Central Andes, Chile (33°-36° SL). Journal of South American Earth Sciences 15 (1): 117-139.

Charrier, R.; Bustamante, M.; Comte, D.; Elgueta, S.; Flynn, J.J.; Iturra, N.; Munoz, N.; Pardo, M.; Theile, R.; Wyss, A.R. 2005. The Abanico extensional basin: Regional extension, chronology of tectonic inversion and relation to shallow seismic activity and Andean uplift. Neues Jahrbuch Fur Geologie Und Palaontologie-Abhandlungen 236 (1-2): 43-77.

Charrier, R.; Pinto, L.; Rodríguez, M.P. 2007. Tectonostratigraphic evolution of the Andean orogen in Chile. *In* Geology of Chile (Moreno, T.; Gibbons, W.;

editors). The Geological Society, Special Publication: 21-114. London.

De Pascale, G.P. 2021. Comment on "Crustal faults in the Chilean Andes: geological constraints and seismic potential" by Santibáñez *et al*. (2019). Andean Geology 46 (1): 32-65. doi: 10.5027/andgeoV46n1-3067.

DeMets, C.; Gordon, R.G.; Argus, D.F.; Stein, S. 1994. Effect of recent revisions to the geomagnetic reversal time scale on estimates of current plate motions. Geophysical Research Letters 21 (20): 2191-2194.

Díaz, D.; Maksymowicz, A.; Vargas, G.; Vera, E.; Contreras-Reyes, E.; Rebolledo, S. 2014. Exploring the shallow structure of the San Ramón thrust fault in Santiago, Chile (~33.5° S), using active seismic and electric methods. Solid Earth 5 (2): 837-849.

Dura, T.; Cisternas, M.; Horton, B.P.; Ely, L.L.; Nelson, A.R.; Wesson, R.L.; Pilarczyk, J.E. 2015. Coastal evidence for Holocene subduction-zone earthquakes and tsunamis in central Chile. Quaternary Science Reviews 113: 93-111.

Estay, N.P.; Yáñez, G.; Carretier, S.; Lira, E.; Maringue, J. 2016. Seismic hazard in low slip rate crustal faults, estimating the characteristic event and the most hazardous zone: study case San Ramón Fault, in southern Andes. Natural Hazards and Earth System Sciences 16 (12): 2511-2528.

Farías, M.; Charrier, R.; Carretier, S.; Martinod, J.; Fock, A.; Campbell, D.; Comte, D. 2008. Late Miocene high and rapid surface uplift and its erosional response in the Andes of central Chile (33-35 S). Tectonics 27 (1): TC1005.

Fock, A. 2005. Cronología y tectónica de la exhumación en el Neógeno de los Andes de Chile central entre los 33° y los 34° S. Memoria de Título (Inédito), Universidad de Chile, Departamento de Geología: 179 p.

Fock, A.; Charrier, R.; Farías; M.; Muñoz, M. 2006. Fallas de vergencia oeste en la Cordillera Principal de Chile Central: Inversión de la cuenca de Abanico (33°-34° S). Revista de la Asociación Geológica Argentina, Publicación Especial 6: 48-55.

Förstner, W.; Pertl, A. 1986. Photogrammetric standard methods and digital image matching techniques for high precision surface measurements. *In* Pattern Recognition in Practice (Gelsema, E.S.; Kanal, L.N.; editors). Noth-Holland: 57-72. Amsterdam.

Giambiagi, L.B.; Ramos, V.A.; Godoy, E.; Álvarez, P.P.; Orts, S. 2003. Cenozoic deformation and tectonic style of the Andes, between 33° and 34° south latitude. Tectonics 22 (4): 1-19.

Gripp, A.E.; Gordon, R.G. 2002. Young tracks of hotspots and current plate velocities. Geophysical Journal International 150 (2): 321-361.

Harris, C.; Stephens, M. 1988. A Combined Corner and Edge Detector. *In* Proceedings of the Alvey Vision Conference: 147-152. Manchester. doi:10.5244/C.2.23.

Lavenu, A. 2006. Neotectónica de los Andes entre 1° N y 47° S (Ecuador, Bolivia y Chile): una revisión. Revista de la Asociación Geológica Argentina 61 (4): 504-524.

Lavenu, A.; Cembrano, J. 2008. Deformación compresiva cuaternaria en la Cordillera Principal de Chile central (Cajón del Maipo, este de Santiago). Revista Geológica de Chile 35 (2): 233-252. doi: 10.5027/andgeoV35n2-a03.

Lavenu, A.; Thiele, R.; Cembrano, J. 1994. Neotectónica compresiva plio-cuaternaria en la Depresión central de Chile. *In* Congreso Geológico Chileno, No. 7, Actas 1: 324-328. Concepción.

Li, Y.G.; De Pascale, G.P.; Quigley, M.C.; Gravley, D.M. 2014. Fault damage zones of the M7.1 Darfield and M6.3 Christchurch earthquakes characterized by fault-zone trapped waves. Tectonophysics 618: 79-101.

Marrett, R.; Allmendinger, R.W. 1990. Kinematic analysis of fault-slip data. Journal of Structural Geology 12 (8): 973-986.

McGill, S.F.; Sieh, K. 1991. Surficial offsets on the central and eastern Garlock fault associated with prehistoric earthquakes. Journal of Geophysical Research: Solid Earth 96 (B13): 21597-21621.

Mosolf, J.G.; Gans, P.B.; Wyss, A.R.; Cottle, J.M.; Flynn, J.J. 2019. Late Cretaceous to Miocene volcanism, sedimentation, and upper-crustal faulting and folding in the Principal Cordillera, central Chile: field and geochronological evidence for protracted arc volcanism and transpressive deformation. Geological Society of America, Bulletin 131 (1-2): 252-273.

Muñoz, M.; Deckart, K.; Charrier, R.; Fanning, M. 2009. New geochronological data on Neogene intrusive rocks from the high Andes of central Chile (33º15'-34º00' S). *In* Congreso Geológico Chileno, No. 12, Actas S8-008: 4 p. Santiago.

Naylor, M.A.; Mandl, G.T.; Supesteijn, C.H.K. 1986. Fault geometries in basement-induced wrench faulting under different initial stress states. Journal of Structural Geology 8 (7): 737-752.

Pardo-Casas, F.; Molnar, P. 1987. Relative motion of the Nazca (Farallon) and South American plates since Late Cretaceous time. Tectonics 6 (3): 233-248.

Pérez, A.; Ruiz, J.A.; Vargas, G.; Rauld, R.; Rebolledo, S.; Campos, J. 2014. Improving seismotectonics and seismic hazard assessment along the San Ramón Fault

at the eastern border of Santiago city, Chile. Natural Hazards 71 (1): 243-274.

Pfiffner, O.A.; Burkhard, M. 1987. Determination of paleostress axis orientations from fault, twin and earthquake data. Annales Tectonicae 1: 48-57.

Piquer, J.; Skarmeta, J.; Cooke, D.R. 2015. Structural evolution of the Rio Blanco-Los Bronces District, Andes of Central Chile: controls on stratigraphy, magmatism, and mineralization. Economic Geology 110 (8): 1995-2023.

Piquer, J.; Berry, R.F.; Scott, R.J.; Cooke, D.R. 2016. Arc-oblique fault systems: Their role in the Cenozoic structural evolution and metallogenesis of the Andes of central Chile. Journal of Structural Geology 89: 101-117.

Piquer, J.; Hollings, P.; Rivera, O.; Cooke, D.R.; Baker, M.; Testa, F. 2017. Along-strike segmentation of the Abanico Basin, central Chile: New chronological, geochemical and structural constraints. Lithos 268: 174-197.

Piquer Romo, J.; Yáñez, G.; Rivera, O.; Cooke, D. 2019. Long-lived crustal damage zones associated with fault intersections in the high Andes of Central Chile. Andean Geology 46 (2): 223-239. doi: 10.5027/andgeoV46n2-3106.

Rauld, R. 2002. Análisis morfoestructural del frente cordillerano de Santiago oriente, entre el Río Mapocho y la Quebrada de Macul. Memoria de Título (Inédito), Universidad de Chile, Departamento de Geología: 57 p.

Rauld, R. 2011. Deformación cortical y peligro sísmico asociado a la falla San Ramón en el frente cordillerano de Santiago, Chile Central (33° S). Ph.D. Tesis (Inédito), Universidad de Chile, Departamento de Geología: 311 p.

Riesner, M.; Lacassin, R.; Simoes, M.; Armijo, R.; Rauld, R.; Vargas, G. 2017. Kinematics of the active West Andean fold-and-thrust belt (central Chile): Structure and long-term shortening rate. Tectonics 36 (2): 287-303.

Schwartz, D.P. 2018. Review: Past and Future Fault Rupture Lengths in Seismic Source Characterization-the Long and the Short of it. Bulletin of the Seismological Society of America 108 (5A): 2493-2520.

Schwartz, D.P.; Coppersmith, K.J. 1984. Fault behavior and characteristic earthquakes: Examples from the Wasatch and San Andreas fault zones. Journal of Geophysical Research: Solid Earth 89 (B7): 5681-5698.

Sellés, D.; Gana, P. 2001. Geología del área Talagante-San Francisco de Mostazal: Regiones Metropolitana y del Libertador General Bernardo O'Higgins. Servicio Nacional de Geología y Minería, Carta Geológica de Chile, Serie Geología Básica 74: 30 p., 1 mapa escala 1:100.000. Santiago.

Sepúlveda, S.A.; Astroza, M.; Kausel, E.; Campos, J.; Casas, E.A.; Rebolledo, S.; Verdugo, R. 2008. New findings on the 1958 Las Melosas earthquake sequence, central Chile: implications for seismic hazard related to shallow crustal earthquakes in subduction zones. Journal of Earthquake Engineering 12 (3): 432-455.

Serey, A.; Sepúlveda, S.A.; Murphy, W.; Petley, D.N.; De Pascale, G.P. 2020. Developing conceptual models for the recognition of coseismic landslides hazard for shallow crustal and megathrust earthquakes in different mountain environments-an example from the Chilean Andes. Quarterly Journal of Engineering Geology and Hydrogeology 54 (2): qjegh2020-023. doi: 10.1144/qjegh2020-023.

Sernageomin. 2003. Mapa Geológico de Chile: versión digital. Servicio Nacional de Geología y Minería, Publicación Geológica Digital, No. 4 (CD-ROM, versión 1.0, 2003). Santiago.

Sibson, R.H. 1977. Fault rocks and fault mechanisms. Journal of Geological Society of London 133: 191-214.

Sylvester, A.G. 1988. Strike-slip faults. Geological Society of America, Bulletin 100 (11): 1666-1703.

Thiele, R. 1980. Hoja Santiago. Instituto de Investigaciones Geológicas, Carta Geológica de Chile 39: 51 p., 1 mapa escala 1.250.000. Santiago.

Thompson Jobe, J.A.; Philibosian, B.; Chupik, C.; Dawson, T.K.; Bennett, S.E.; Gold, R.; Pierce, I. 2020. Evidence of previous faulting along the 2019 Ridgecrest, California, earthquake ruptures. Bulletin of the Seismological Society of America 110 (4): 1427-1456.

Vargas, G.; Klinger, Y.; Rockwell, T.K.; Forman, S.L.; Rebolledo, S.; Baize, S.; Lacassin, R.; Armijo, R. 2014. Probing large intraplate earthquakes at the west flank of the Andes. Geology 42 (12): 1083-1086.

Wall, R.; Sellés, D.; Gana, P. 1999. Mapa Geológico del Área Til-Til-Santiago. Servicio Nacional de Geología y Minería, Mapas Geológicos 11, 1 mapa escala 1.100.000. Santiago.

Wells, D.L.; Coppersmith, K.J. 1994. New empirical relationships among magnitude, rupture length, rupture width, rupture area, and surface displacement. Bulletin of the Seismological Society of America 84 (4): 974-1002.

Wilcox, R.E.; Harding, T.P.; Seely, D.R. 1973. Basic wrench tectonics. American Association of Petroleum Geologists Bulletin 57: 74-96.

Woodcock, N.H.; Fischer, M. 1986. Strike-slip duplexes. Journal of Structural Geology 8 (7): 725-735.

Manuscript received: November 27, 2018; revised/accepted: March 29, 2019; available online: May 31, 2021.